Chapter 8

1D Photonic Crystals: Principles and Applications in Silicon Photonics

Liangshun Han

Additional information is available at the end of the chapter

http://dx.doi.org/10.5772/intechopen.71753

Abstract

One-dimension (1D) photonic crystals have been widely used in silicon photonics due to its simple structure and multiple working regimes: diffraction, Bragg reflection, and sub-wavelength regimes. Thanks to recent development of photonic technologies and high-resolution lithography, many 1D photonic crystal-assisted silicon integrated devices have been proposed and demonstrated to further increase integration density and improve device performance. This chapter first presents some fundamentals of 1D photonic crystals. An overview of the applications of 1D photonic crystals in silicon photonics is then given including grating couplers, waveguide crossings, multimode interference couplers, polarization-independent directional couplers, hybrid lasers, polarizers, and high-order mode filters, among others. Particular attention is paid to providing insight into the design strategies for these devices.

Keywords: photonic crystals, diffractive gratings, sub-wavelength gratings, Bragg gratings, silicon photonics

1. Introduction

Extensive research has been performed to realize large-scale integration of silicon photonics for optical communication networks [1, 2], optical computing [3, 4], and biosensing [5, 6]. The impetus of this research lies in the fact that silicon-on-insulator (SOI) technology is fully compatible with complementary metal oxide semiconductor (CMOS) technology and possesses high refractive index contrast enabling compact devices. Recent efforts in silicon photonic devices, such as III–V/silicon hybrid lasers [7–9], modulators [10, 11], photodetectors [12], and switches [13, 14], have all paved a path toward realizing silicon-based high-density electronic and photonic integration circuits (EPICs) [15]. However, due to high-index contrast, photonic

devices based on SOI waveguides always suffer from some issues including high polarization sensitivity, limited bandwidth, sever phase errors caused by fabrication, thermal sensitivity, and relatively large loss. Those issues greatly limit application range of silicon-based photonic devices. There has been considerable effort by the international community to improve device performances by designing new structures, introducing new materials, combining different effects, developing new fabrication processes, discovering new functionalities, etc. The application of 1D photonic crystals in silicon photonics is a representative example.

1D photonic crystals are the simplest structure in photonic crystal family [16]. Interestingly, 1D photonic crystals still possess many exciting properties such as adjustable dispersion and birefringence, acting as homogeneous materials. Compared with 2D or 3D photonic crystals, the simple structure of 1D photonic crystals makes them easy to be integrated with the existing photonic devices without changing fabrication procedures. Consequently, many high-performance silicon-based devices have been proposed and demonstrated by exploiting those exciting properties of 1D photonic crystals. This chapter aims to provide the readers with some fundamentals of 1D photonic crystals and present an extensive overview of their applications in silicon photonics. The chapter is organized as follows. Section 2 describes the fundamentals of 1D photonic crystals. For the sake of clarity, the overview of their applications is divided into three sections (Sections 3–5) on the basis of three operating regimes.

2. Fundamentals of 1D photonic crystals

In silicon photonics, the 1D photonic crystals can be formed by periodic strip structures as shown in **Figure 1**. Normally, those strips are high-index crystal silicon layer which is optical waveguide core layer as well. The high-index strips are surrounded by low-index material such as air, silicon oxide, and polymer to form a periodically modulated refractive index distribution. In general, the incident direction of light could be any direction relative to photonic crystals. In practical terms, two special cases are widely employed: (a) light propagates crosswise through the 1D photonic crystal (propagation along the y- or z-axis in **Figure 1**), and (b) light propagates lengthwise through the 1D photonic crystal (propagation along the x-axis in **Figure 1**). In this chapter, we will focus on lengthwise periodic structures since lengthwise structures can be easily integrated with sub-micrometer

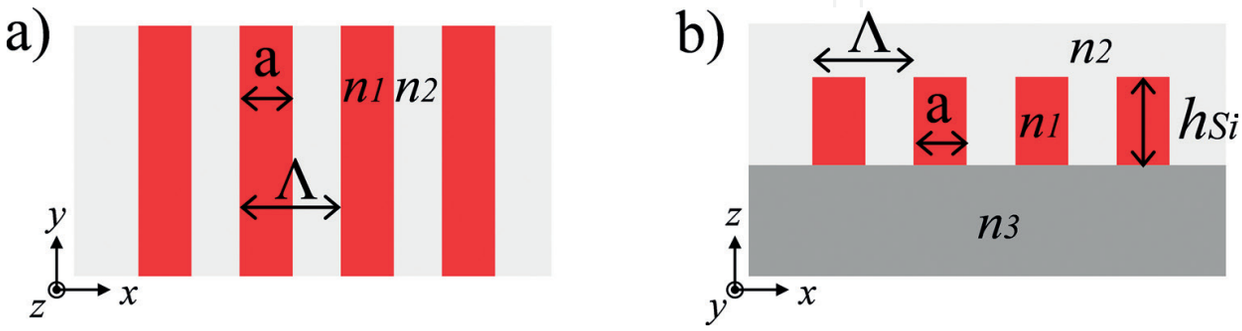

Figure 1. (a) Top view and (b) cross section of a 1D photonic crystal.

http://dx.doi.org/10.5772/intechopen.71753

silicon waveguides and provide more flexibilities than that of crosswise periodic structures. Nowadays, extensive review papers and books are available for fully understanding the specific electromagnetic properties of the periodic structures considered here [16]. However, to provide intuitive guidelines for the design process, a much simpler theory will be used in this chapter.

A lengthwise 1D photonic crystal shown in **Figure 1** generally operates in the following three regimes, depending on the ratio between the structure's pitch (Λ) and the operating free-space wavelength (λ):

i. Diffraction regime. The incoming beam is scattered in different orders.

ii. Bragg reflection regime. The incoming beam is reflected backward.

iii. Sub-wavelength regime. The diffraction and reflection effects due to the periodicity of the structure are suppressed.

Figure 2 shows a schematic k–ω diagram of a 1D periodic structure with lengthwise propagation (along the x-axis) [16]. One can see that, for a given pitch periodic structure, the working regime is strongly related to free-space operating wavelength λ or operating frequency ω. When $\omega > \omega_2$ (above the first photonic bandgap), the waveguide becomes lossy for Bloch mode, and the light will be radiated out of the waveguide. This character has been utilized to design fiber-to-chip surface couplers (grating couplers). In the frequency range of $\omega_2 > \omega > \omega_1$ (the first photonic bandgap), light cannot propagate through the periodic structure and is reflected, and this is Bragg reflection regime. The propagation constant in this regime is

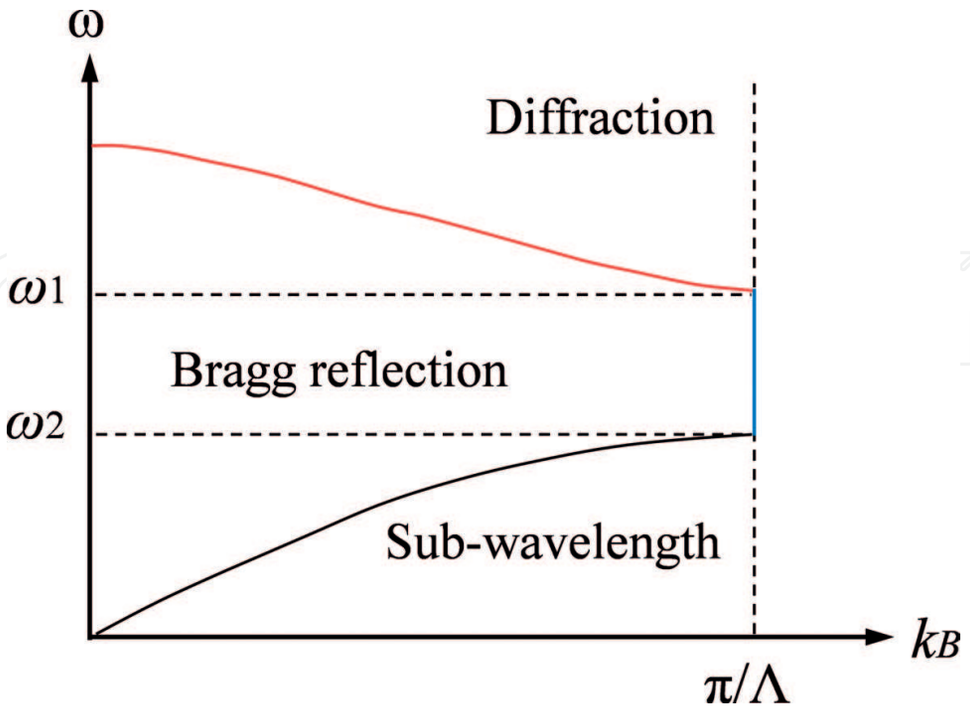

Figure 2. The schematic band diagrams a 1D photonic crystals with lengthwise propagation (along the x-axis).

constant: $k_B = \pi/\Lambda$. The bandgap has been extensively exploited to design distributed Bragg reflectors (DBRs) on different photonic platforms.

The last regime is located below the first photonic bandgap where the operating frequency is smaller than ω_1. From **Figure 2**, one can find that the propagation constant k_B grows monotonically as operating frequency increases, indicating that the periodic waveguide behaves as a conventional waveguide. Thus, in sub-wavelength regime, periodic structures work as homogeneous media. Consider a general case, light propagates (along the x-axis) through the structure (shown in **Figure 1**), with a linear polarization either parallel ($E_\parallel$) or perpendicular ($E_\perp$) to the interfaces between the two media. The equivalent effective index of the structure can be expressed with the zeroth-order approximation [17]:

$$n_\parallel^2 = \frac{w}{\Lambda} n_1^2 + \frac{\Lambda - w}{\Lambda} n_2^2 \tag{1}$$

$$\frac{1}{n_\perp^2} = \frac{w}{\Lambda} \frac{1}{n_1^2} + \frac{\Lambda - w}{\Lambda} \frac{1}{n_2^2} \tag{2}$$

where w/Λ is duty cycle of the structure. Thus, both effective index and effective birefringence can be engineered by adjusting the geometry of the structure. This allows for completely new design approaches and can be exploited in a variety of devices. Eqs. (1) and (2) also apply to crosswise structures.

3. Applications of diffraction regime

For the sake of clarity, the discussion on the applications of 1D photonic crystals in silicon photonics is divided into three parts. Hereinafter, we will use the general expression "diffractive gratings" and "sub-wavelength gratings (SWG)" to indicate the 1D photonic crystals operating in diffraction regime and in sub-wavelength regime, respectively. This section is devoted to applications of the diffraction regime. Applications of sub-wavelength regime and Bragg reflection regime are discussed in Sections 4 and 5, respectively. This section focuses on the key components in silicon photonics: grating couplers. To further improve the performance, combination of diffractive gratings and crosswise sub-wavelength structures is also presented.

A grating coupler is a 1D periodic structure that can diffract light from propagation in the waveguide (in plane) to free space (out of plane). By placing an optical fiber above the chip, part of the radiated light is collected. It is normally used as an I/O device to couple light between fiber and sub-micrometer silicon waveguides. And, grating couplers are defined lithographically and can be placed anywhere on the chip surface to enable inputs and outputs, which are particularly useful for massive production. **Figure 3** shows the cross section view of a shallow-etched grating coupler on a SOI wafer. The thickness of the core silicon layer and the thickness of the buried oxide (BOX) layer are determined by the wafer type. Normally, the thickness of core silicon layer (h_{Si}) is 150–300 nm. The cladding material is usually air ($n_2 = 1$), silicon dioxide, or an index-matching liquid ($n_2 \sim 1.45$).

http://dx.doi.org/10.5772/intechopen.71753

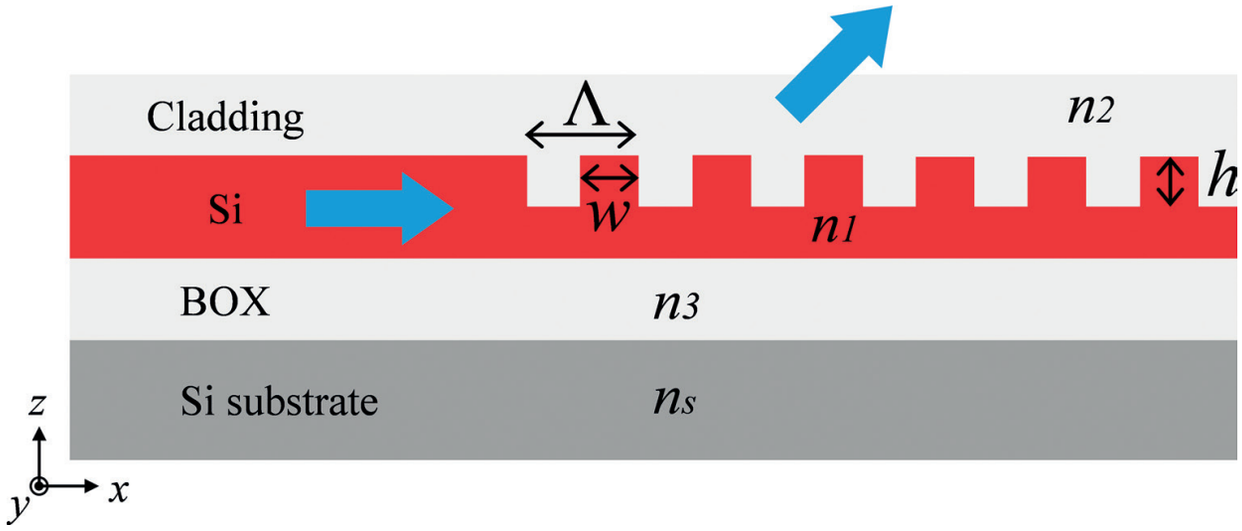

Figure 3. The cross section view of a shallow-etched grating coupler.

Figure 4 illustrates the concept of a grating coupler working as an output coupler. The operation of a grating coupler can be understood by the constructive and destructive interference arising from the wave fronts generated by the diffraction of light from the grating strips [18, 19]. First, we can check **Figure 4a**. In this case, the operating wavelength matches the pitch of the gratings. The first-order diffraction will vertically propagate, and the second-order diffraction will be back to the waveguide. However, the back-traveling light will be considered as reflection for the silicon waveguide, which is undesired since the light path between two grating couplers can form a Fabry-Perot oscillation cavity. This oscillation will modulate the transmission of other components. One efficient way to address this issue is detuning the grating and tilting the fiber (see **Figure 4b**) with a small angle to the grating surface. When the wavelength inside waveguide is smaller than the pitch of the gratings, the diffracted light waves will propagate at an angle, and reflection caused by second-order diffraction will be strongly suppressed.

The grating coupler could be well described by Bragg Law. If the grating parameters are fixed as constants (such as pitch and refractive indices of layers), then the radiation angle is given by the equation [18]:

$$n_2 \sin\theta_k = n_{eff} + \frac{k\lambda}{\Lambda} \tag{3}$$

where n_2 is the refractive index of the cladding material (see **Figure 3**) and k is an integer which represents the diffraction order. In some literatures, the effective index n_{eff} is substituted by Bloch-Floquet mode index (n_B). The main reason is that the relatively short light extraction length between a fiber and a grating coupler generally causes a strong perturbation in the waveguide. But for preliminary design process, using effective index is enough to qualitatively understand the property. In Ref. [18], only when $\sin\theta_k$ is real, the gratings diffract light from the waveguide. Consequently, we can play with the pitch of gratings so that only the order $k = -1$ occurs or dominates.

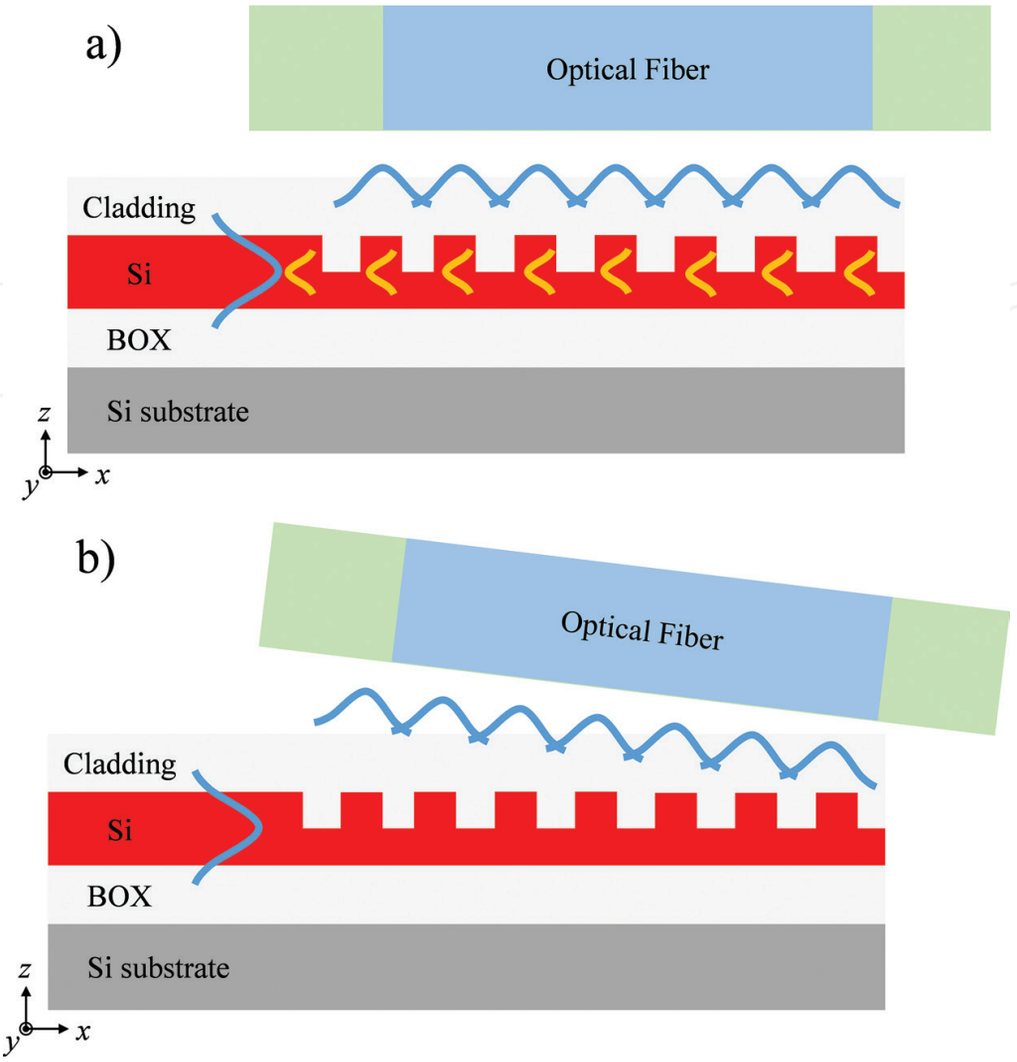

Figure 4. Diagrams describing the concept of a grating coupler working as an output coupler. (a) Vertical first-order diffraction and backward second-order diffraction and (b) tilted first-order diffraction without second-order diffraction.

A straightforward way to realize a grating coupler is using straight gratings connected to a taper to convert the fiber mode to a narrow waveguide mode. To obtain high conversion efficiency, the taper length needs to be more than 100 μm [19–21], which is undesirable for compact and high-density integration schemes. Alternatively, confocal gratings enable more compact designs. The whole grating is shaped to an ellipse with a common focal point, which coincides with the optical focusing point where the single-mode silicon waveguide is connected [22, 23].

One vital property of grating couplers is coupling efficiency. There are three main factors that contribute to a reduced efficiency of a grating coupler:

i. Penetration loss, that is, the fraction of waveguide power that escapes into the substrate. For a shallow-etch structure, there is about 30% of power lost in the substrate; and the penetration loss can be more than 50% in a full-etch structure [19]. This can be improved by using reflectors imbedded in the substrate [24–26]. As a result, the upward radiated

optical power is improved, and radiation downward the substrate is reduced. Those reflectors can be a metal layer or multiple-layer-distributed Bragg reflector.

ii. Back reflection, that is, the optical power reflected from the coupler into the waveguide. For a well-designed shallow-etched grating coupler, the back reflection is less than -20 dB, so this does not contribute a significant loss to the coupler. However, this loss can be much higher in a full-etched grating coupler. Coupling the light under a small angle also helps to eliminate the first-order Bragg reflection, which is another reason why grating couplers are often designed with a coupling angle.

iii. Mode mismatch, that is, the overlap integral between the diffracted light beam and the near-Gaussian optical fiber mode [27]. In theory, the overlap integral is determined by the fraction of waveguide power diffracted from each pitch of the gratings. Approximately, this fraction is in direct proportion to refractive index difference between the strips of the gratings and the grooves. Therefore, in comparison with full-etched structures, a shallow-etched structure possesses a lower index difference which produces a relative wide radiated light beam. Consequently, conventional grating couplers with shallow-etched gratings help enhancing the field overlap.

It is should be noted that the power loss caused by mode mismatch can be further improved by apodizing or chirping the gratings [20, 28, 29] in which the index difference is varied along the structure to obtain a radiated beam that resembles the optical fiber mode. Duty cycle varied crosswise SWG structures can also enable the design of apodized grating couplers fabricated by a single, full-etch step. Consider a crosswise SWG structure enabled grating coupler shown in **Figure 5**. x direction is the in plane propagation direction of a conventional grating coupler, and the original grooves are occupied by crosswise SWG structures acting as artificial homogeneous media. The equivalent index of SWG can also be approximately estimated by Eqs. (1) and (2). Thereby, a grating can be apodized by varying the duty cycle (w_y/Λ_y) of the SWG structure located in each groove. However, the introduction of crosswise SWG structures also causes a variation of the radiation angle θ along the grating. To compensate

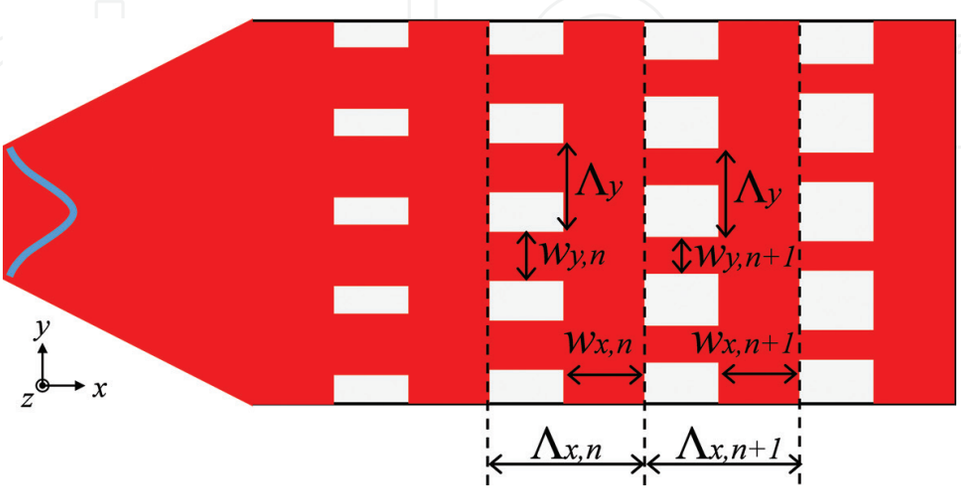

Figure 5. Top view of an apodized grating coupler with crosswise SWG structures.

this variation, chirping the grating along x direction is necessary. An apodized grating coupler with focusing design exhibiting a coupling efficiency of −1.8 dB was reported in Ref. [30].

The combination of diffractive gratings and crosswise SWG structures is also exploited to obtain polarization-independent grating couplers [31, 32]. Conventional grating couplers are highly polarization sensitive, which can be used as polarization filters or polarizers. The effective index in the grating region is highly birefringent, causing different radiation angles for TE and TM polarization states. When we consider a grating coupler with SWG structures shown in **Figure 5**, the effective index of the TE (z-polarized) mode will be much larger than that of the TM (y-polarized) mode in the silicon slab regions. However, in the sub-wavelength regions, from Eqs. (1) and (2), it was found that the effective index of the TE mode $n_{\perp}$ is smaller than that the TM mode $n_{\parallel}$. It is possible to design grating region so that these two effects cancel each other resulting in an identical Bloch mode effective index for both polarization states. Consequently, the grating coupler becomes polarization independent. Ref. [32] demonstrated a similar design possessing a coupling efficiency of −6.5 dB for both polarization states.

Broadband grating couplers with SWG structures were also proposed and demonstrated. A grating coupler with a bandwidth of ~100 nm and a coupling efficiency of −5.6 dB was presented in Ref. [33]. A simulated bandwidth of ~300 nm and a coupling efficiency of −2.8 dB were obtained by employing fully etched triangular holes in Ref. [34].

4. Applications of sub-wavelength regime

This section further presents applications of lengthwise SWG structures in which light propagates perpendicularly to the interfaces of the structure (along the x direction in **Figure 1**). As mentioned in Section 2, it is possible to engineer both effective index and effective birefringence which can be exploited in many silicon photonic devices for optical bandwidth and polarization-sensitivity improvement. In this section, we first discuss the mode convertor between SWG-based waveguides and conventional waveguides, which is the basic component for integration of these two kinds of technologies. Then, we move to some other key components such as waveguide crossings, multimode interference (MMI) couplers, and wideband and polarization-independent directional couplers.

4.1. Mode converters

To fully utilize the properties afforded by SWG-based waveguides and other components, integration and interconnect with conventional waveguides are needed. There are two key points to design such mode converters: low loss and low reflection. To attain both targets, several works have been done in theories and experiments [35, 36]. **Figure 6** shows the schematic diagram of a mode converter which contains three parts: conventional waveguide section, transition section between conventional waveguide and SWG-based waveguide, and SWG-based waveguide section. The transition section determines the performance of this mode converter; a clear approach is chirping the pitch and duty cycle and incorporating bridging

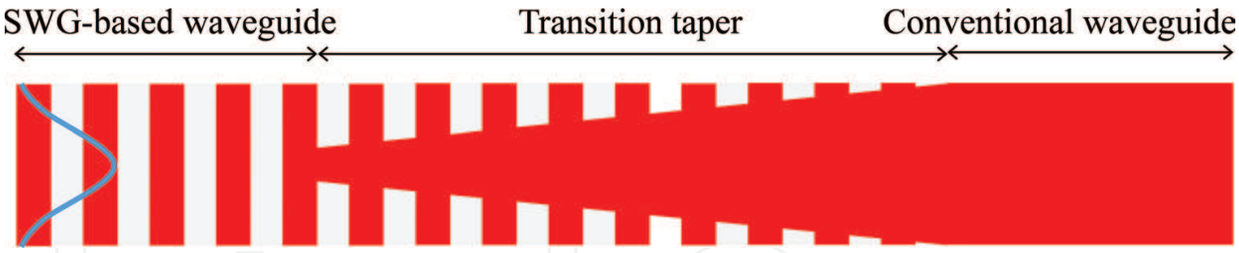

Figure 6. Top view of a SWG-based mode converter with section indications.

elements between the two waveguide sections [36]. Similar to conventional inverse taper, the mode effective index in transition section also gradually changes along propagation; thus, particular care should be taken for avoiding Bragg reflection regime within target operating optical bandwidth.

Mode converters can also be used for fiber-to-chip coupling [35, 37] and coupling between continuous fields and discretized fields [38]. For fiber-to-chip coupling applications, mode converter is carefully designed to match the on-chip waveguide mode size, shape, and effective index to that of a single-mode fiber, thereby increasing coupling efficiency. The insertion loss of such mode converter was extracted from experiments: −0.23 dB for TE mode and −0.47 dB for TM mode [38]. The application for coupling between continuous fields and discretized fields can be found in arrayed waveguide grating (AWG). In an AWG, the main loss and backward reflection are from transition between the slab waveguide (where continuous fields are from) and the array waveguides (where discretized fields appear). The loss is from the gap between arrayed waveguides, and reflection is caused by high-index difference between slab region and free propagation region. By placing well-designed SWG structures between arrayed waveguides, the index difference and fields coupling can be further optimized. Ref. [39] shows some experimental results about AWGs with SWG-based mode converters.

4.2. Waveguide crossings

An efficient waveguide crossing is highly desired to materialize the full potential of silicon photonics for on-chip optical interconnects. Due to the high-index contrast of the silicon platform such as SOI, the insertion loss of a conventional waveguide crossing is around 0.15 dB. To reduce optical loss, waveguide crossing designed by using particle swarm optimization has been proposed and demonstrated, with a loss of −0.028 ± 0.009 dB for 1550 nm operating wavelength [40]. In this part, we introduce some waveguide crossing designs assisted by SWG structures. The experimentally confirmed insertion loss is comparable with or even lower than that of particle swarm-optimized designs. A further advantage of using SWG structures is improving optical bandwidth and polarization sensitivity.

First, we go through some fundamentals of conventional waveguide crossings. **Figure 7a** gives the top view of a conventional waveguide crossing, and cross section of the multimode waveguide region is shown in **Figure 7b**. A conventional design is composed of MMI regions, single-mode access waveguides, and a crossing section. It was found that the intrinsic loss of such design is attributed to three aspects:

i. Phase error in the MMI region. When wide multimode waveguides are utilized, it is possible to find more than two modes excited in MMI regions. Some phase errors will appear, and the perfect self-imaging position cannot be found by adjusting MMI length. To avoid exciting high-order modes, narrow multimode waveguides supporting three modes (fundamental, first order, and second order) are applicable. Among these modes, only fundamental and second-order modes are excited in an symmetric interference MMI structure. Then, the self-imaging length is only related to two modes, and high-order mode phase errors could be thoroughly eliminated.

ii. Loss caused by sharp transitions between single-mode waveguides and MMI regions. As suggested by [41], a linear or nonlinear taper can be applied to reduce the transition loss. It is worth to underline that the taper also affects the power portion in the second-order mode in MMI regions [42]. Through simulation, we can find the optimal power ratio between fundamental mode and second-order mode. If the power ratio is too small, the MMIs even lose the capability of focusing light beam at the center of the crossing section, causing mode mismatch between the diverged beam after passing through the crossing section and the guided modes of the multimode waveguide. When the power ratio is larger than the optimal value, a large amount of the second-order mode possessing a wide angular spectrum scatters through the crossing section, and some of it radiates into the orthogonal MMI regions, resulting in substantial loss and crosstalk. Consequently, when choosing the length of the taper, a trade-off between modal transition loss and two-mode power ratio needs to be found.

iii. Mode mismatching between multimode waveguides and the crossing section. The crossing section is much wider than the multimode waveguide width, which can be considered as a slab waveguide that supports pure TE modes. However, the mode in the single-mode access waveguide and the second-order mode in the multimode waveguide are both quasi-TE modes with a considerable amount of TM polarization. Then, the TM mode power will be dissipated in the crossing section. It is found that the power portion of TM polarization can be effectively suppressed by increasing the lateral cladding index (n_{lc}) in MMI regions. One straightforward way is depositing a high-index material such

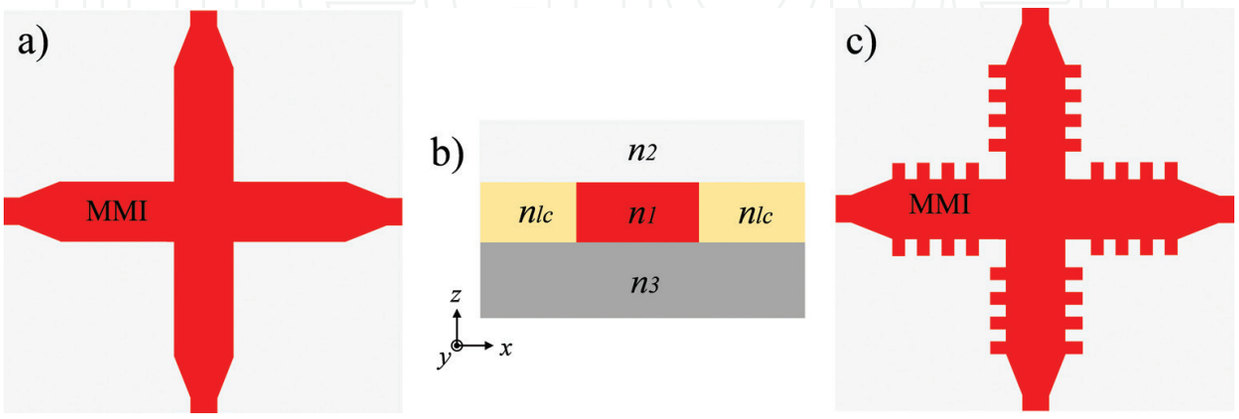

Figure 7. (a) Top view of a conventional waveguide crossing, (b) cross section view of MMI sections, and (c) top view of a SWG-assisted waveguide crossing design.

as Si_xN_{1-x}. Also, using a tightly controlled shallow-etched structure is feasible. Both approaches complicate the fabrication process.

In Ref. [42], researchers developed a new waveguide crossing assisted by SWG structures to engineer the lateral cladding index, simplifying fabrication procedures. **Figure 7c** gives the schematic of such design. A 101 × 101 MMI crossing matrix was demonstrated on the SOI platform. An insertion loss of 0.019 dB and a crosstalk lower than −40 dB at 1550 nm operating wavelength were obtained for each crossing. It is worth to note that the optical bandwidth (90 nm) is wider than that of conventional designs.

Figure 8 shows another waveguide crossing design that lies on SWG-based waveguides [43]. In comparison with the designs shown in **Figure 7a** and **7c** this waveguide crossing has no multimode waveguides. At the center of the crossing, a squared segment is used to enable a symmetrical structure. Loss per crossing was measured as 0.023 dB with polarization dependent loss of <0.02 dB and crosstalk below −40 dB [43]. An improvement from this design is polarization insensitivity. More discussions can be found in Ref. [43].

4.3. MMI couplers

MMI couplers are widely used as basic building blocks in many advanced photonic devices including MZ modulators [10], polarization-handling devices [44], mode handling devices [45, 46], etc. Before reviewing some high-performance MMI coupler assisted by SWG structures, we will briefly recall the fundamental limitations of conventional MMI couplers.

A MMI coupler consists of single-mode in−/output waveguides and a multimode waveguide section, as shown in **Figure 9**. The input light beam excites multiple modes in the central section with different excitation coefficients. The coefficients are determined by input mode profile and the structure of the central section (MMI section). Those modes propagate through the central section with different propagation constants (β_m) and interfere with each other to form the N-fold self-imaging of the input mode [47]. Placing output waveguides at the imaging position, beam splitting and combining function can be achieved. The MMI or central section length (L_{MMI}) has a certain relationship with beat length (L_π) of the two lowest excited modes in the central section. The beat length at operating wavelength is given by

$$L_\pi = \frac{\pi}{\beta_1(\lambda) - \beta_2(\lambda)} \tag{4}$$

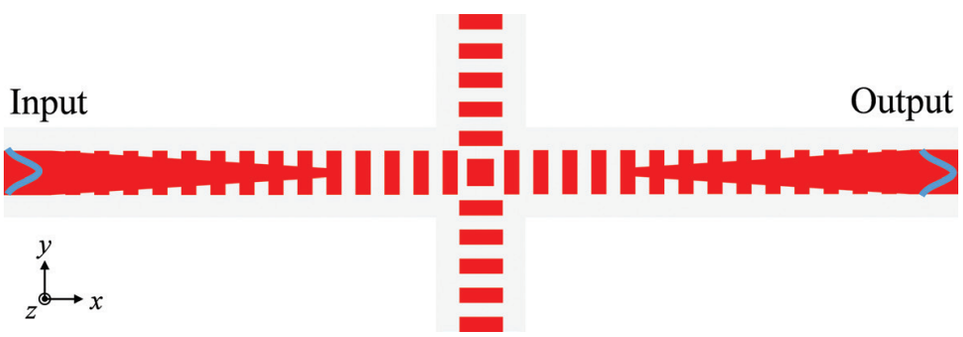

Figure 8. Top view of a SWG-based waveguide crossing.

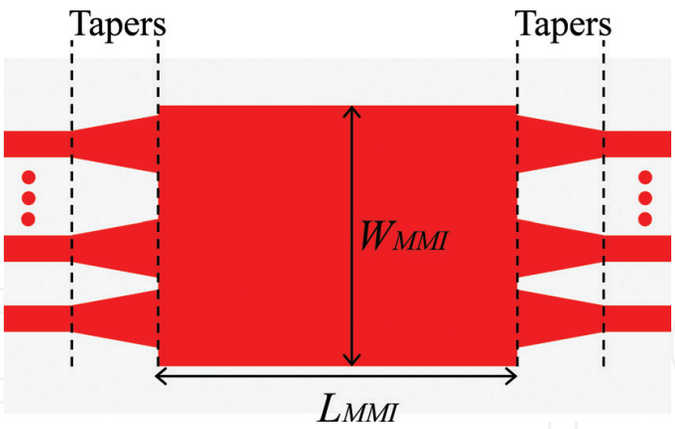

Figure 9. Schematic of a MMI coupler with indications.

Furthermore, to obtain clear images for low loss and power imbalance of MMI couplers, the propagation constant of each excited mode needs to meet the following relation:

$$\beta_m = \beta_1 - \frac{(m^2 - 1)}{3 L_\pi} \pi \tag{5}$$

where m is the mode order and β_1 is the propagation constant of the lowest-order mode. Unfortunately, this condition is only satisfied for the lower order modes, which causes MMI's phase error and excess loss. An obvious approach is to suppress excitations of higher order modes, which can be done by increasing modal width of input mode and reducing the number of modes that MMI supports. Inserting tapered input waveguides between single-mode waveguides and the central section (as shown in **Figure 9**) in return increases modal width ratio between input mode and the excited fundamental mode, resulting in a limited number of (the lower order) modes excited. About reducing supported modes in the central section, reducing the width of MMI section (same effect as that of the use of tapered input) and increasing lateral cladding index (decrease core-cladding refractive index contrast) are feasible methods.

In Eq. (4), the beat length is described only for a certain wavelength. We rewrite the equation as

$$L_\pi = \frac{\lambda}{2(n_1(\lambda) - n_2(\lambda))} \tag{6}$$

It can be seen that the beat length decreases with increasing wavelength. This is the major limitation of the bandwidth of a MMI coupler. To achieve broadband MMI couplers, we need to find a way to suppress high-order modes excited in MMI section and keep $(n_1(\lambda) - n_2(\lambda))$ increasing as wavelength increases.

Now, we review two high-performance MMI couplers assisted by SWG structures. The first case is 4 × 4 MMI coupler serving as a 90° hybrid for coherent detections. One vital parameter of this MMI coupler is phase error. As discussed before, the use of input taper is a common practice to obtain small phase errors. But for SOI platform, only using input taper is not enough to meet the target since the large core-cladding index contrast in SOI waveguides

leads higher-order modes to not properly fulfill Eq. (4). The large lateral index contrast can be tailored by an (some) extra shallow-etch step(s) to define shallow-etched multimode region. This was experimentally confirmed as an efficient way [48]. However, extra etch steps and tightly controlled etching depth are required, complicating the fabrication process and not suitable for massive production. Instead of introducing shallow-etch process, laterally integrating SWG structures also allows for lateral cladding index engineering with single full-etch step. The design process is straightforward: (1) calculate the equivalent effective index of SWG structures under different pitch and duty cycles; (2) sweep the cladding index of a 4 × 4 MMI coupler to find an optimum value; (3) use the data calculated in Step 1 as a lookup table and, then, geometry parameters of the sub-wavelength structure that yields the desired value of lateral cladding index can be found; and (4) use FDTD to further verify the structure. The schematic diagram is depicted in **Figure 10a**. Simulated common mode rejection ratio and phase error of less than 24 dBe and 2°, respectively, are presented in Ref. [49]. This technology can be also exploited in any $N \times N$ MMI coupler.

The second case is broadband 2 × 2 MMI coupler. In practices, broadband MMI couplers are demanded to simplify system and reduce cost. Similar to the above case, optimization of tapered input broadens the bandwidth. In Ref. [50], researchers proposed a broadband 2 × 2 MMI coupler in which the conventional multimode section is replaced with a lengthwise SWG-based waveguide of 6.0 μm width, 198.0 nm pitch, and 50% duty cycle. The schematic diagram is shown in **Figure 10b**. To fully understand how the SWG structures can be exploited to significantly increase the bandwidth of MMI couplers, it is useful to replot the sub-wavelength regime in **Figure 2** in an equivalent way as shown in **Figure 11**. One can see that the sub-wavelength regime can be divided into two regions: high dispersion region (λ is close to Bragg wavelength) and low dispersion region ($\lambda >> \Lambda$). The exciting part is that the dispersion value is adjustable through changing pitch, which can be utilized to design broadband MMI couplers. In results, the bandwidth of the MMI coupler in **Figure 10b** is determined by the pitch. To connect with conventional waveguide structures, mode converters similar as the one described in Section 4.1 were placed at in−/output ports as shown in **Figure 10b**. The mode converters also help to expand mode field to excite only lower-order modes. Due to the relatively low equivalent refractive index of the SWG-based multimode region, the MMI length is also shortened in return. Additionally, this technology can be applied to design broadband directional couplers [51].

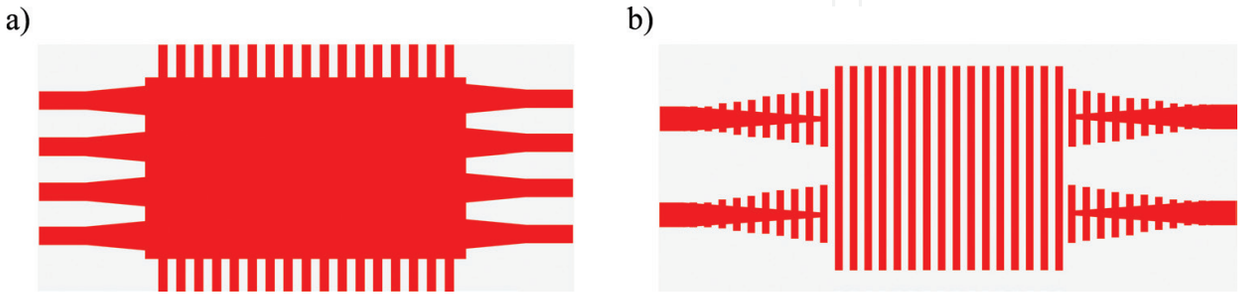

Figure 10. Schematics of MMI couplers: (a) a 4 × 4 MMI coupler with lateral SWG structures and (b) a 2 × 2 MMI couplers with SWG-based multimode section.

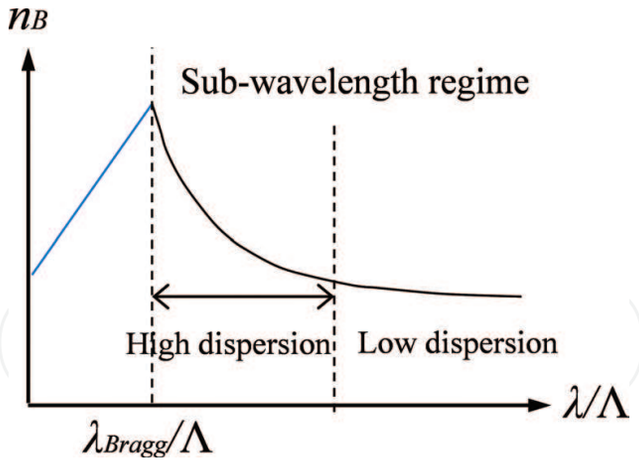

Figure 11. Dispersion in sub-wavelength regime.

Figure 12. Schematic of a polarization-independent directional coupler based on slot waveguides with SWG structures.

4.4. Polarization-independent directional couplers

With its superior performances, directional coupler (DC) has attracted considerable attentions and been widely used in many applications, including on-chip sensors, filters, switches, and polarization beam splitters. In comparison with other couplers, such as MMI couplers and Y-branch couplers, DCs process valuable properties in terms of ultra-low loss, low reflection, and arbitrary power coupling ratio obtained by adjusting the length and gap of the coupling region. However, by using sub-micrometer SOI waveguides, the beat length of TE mode greatly differs from that of TM mode due to the high birefringence of silicon waveguides, resulting in power ratio sensitivity to polarization states. Polarization-independent DC is useful for some applications where the amount of collected or split optical power is concerned. Some techniques have been proposed and experimentally confirmed to address this issue. One solution is to use polarization diversity schemes where polarization splitting and rotating devices are needed, which increases system size and complexity. Another approach is to make the directional coupler inherently polarization insensitive [52–54].

Recently, a SWG-assisted slot waveguide polarization-independent DC with relatively large fabrication tolerance has been demonstrated on SOI chip [55]. **Figure 12** describes the schematic diagram of this design. The SWG structures are extended into the gap between two parallel slot

waveguides. The SWG structures are considered as homogenous media. By calculating the relation between beat length of both polarization states and refractive index of SWG structures (n_k), it was found that the two curves are of different slopes. By adjusting the duty cycle, if the effective indices of the TE mode $n_{\perp}$ and TM mode $n_{\parallel}$ in SWG structures meet the n_{kTE} and n_{kTM} for same beat length for TE and TM modes, then the optimum duty cycle is attained. FDTD simulations for further confirmation are necessary. The measured coupling efficiency is 97.4 and 96.7% for TE and TM modes, respectively, at a wavelength of 1550 nm. It is worth noting that an additional advantage of this design is its wide bandwidth over 120 nm (1475–1595 nm) theoretically and exceeding the entire C-band (1525–1570 nm) experimentally. To interconnect such design with a conventional waveguide, a slot-to-strip waveguide converter is required.

5. Applications of Bragg reflection regime

This section is devoted to applications of Bragg reflection regime of 1D photonic crystals. For the sake of clarity (unless otherwise stated), hereinafter we will use the general expression "Bragg gratings" to indicate the 1D photonic crystals operating in Bragg reflection regime as shown in **Figure 2**. One prominent feature of Bragg gratings is the linear relation $n_{Bragg} \sim \lambda/\Lambda$ within the photonic bandgap ($\omega_1 > \omega > \omega_2$). The bandgap has been extensively exploited to design DBRs on different photonic platforms as key elements of DBR lasers [56, 57], distributed feedback (DFB) lasers [58, 59], fiber Bragg gratings (FBGs) [60], VCSELs [61], etc. On silicon platform, silicon waveguide-based Bragg gratings have been integrated with III–V gain elements to provide optical feedback for lasers on a silicon chip.

This section starts with a brief discussion of Bragg gratings serving as mirrors in hybrid lasers on a silicon chip (Section 5.1). Section 5.2 is dedicated to Bragg gratings designed as a polarizer and higher-order mode pass filter.

5.1. Hybrid lasers with Bragg gratings

The realization of an efficient, reliable, and electrically pumped laser on a silicon wafer is still a scientific challenge. In Ref. [15], researchers first demonstrated a high-performance electrically pumped quantum-dot laser through epitaxial growth of III–V materials on a silicon substrate. Another common-practice approach to realize light source on a silicon wafer is wafer bonding. Several bonding process schemes have been proposed [9, 62–66]. To fabricate a single-wavelength laser and multiwavelength laser array, prefabricated single-wavelength laser diodes can be directly bonded on a silicon wafer [62]. Alternatively, embed III–V gain sections to silicon photonic circuits and the wavelength-selections are done by some silicon-based wavelength-sensitive devices such as ring resonator, slotted feedback structure, and Bragg reflector. In Ref. [66], a four-channel multiwavelength DFB evanescent laser array was designed and fabricated. Beneath each III–V gain section, Bragg gratings were fabricated on the surface of the silicon waveguide. The ASE from a gain section propagates and evanesces into a silicon waveguide and is modulated by gratings, forming a DFB laser. For realizing different channel wavelengths, the width of silicon waveguide is varied to obtain different Bragg propagation constants.

5.2. TM-pass polarizers

Photonic devices based on SOI waveguides always suffer from severe polarization-sensitivity problems due to high birefringence, which greatly limits their application range. Various polarization-handling devices have been attracting attentions, including polarization beam splitters, polarization rotators [67], and polarizers. Among them, a polarizer is used to achieve linearly polarized light with a high extinction ratio. In practices, a low loss, high extinction ration, and compact footprint polarizer is highly desired. Many designs have been proposed and demonstrated on silicon wafers [68–70]. The basic rationale of designing a polarizer is to lose or filter unexpected polarization state out from the optical propagation paths with negligible effect on desired polarization state and maintain the device size as small as possible.

In Ref. [71], a waveguide-based TM-pass polarizer is fabricated with 1D photonic crystals. The schematic of this design is depicted in **Figure 13**. The device is composed of three parts: in−/output waveguides, 1D photonic crystal with teeth and bridges, and transition tapers. The pitch was well designed to make the waveguide supporting Bloch mode for TM polarization state, so that the incident TM-polarized light goes through the waveguide with very low excess loss. On the other hand, for TE polarization state, the waveguide works as a Bragg reflector, and consequently the incident TE-polarized light is reflected with very high efficiency. Therefore, the following conditions should be satisfied approximately [71]:

$$n_b^{TE}(\Lambda - w) + n_{ac}^{TE} w \;=\; \lambda/2 \tag{7}$$

$$n_b^{TM}(\Lambda - w) + n_{ac}^{TM} w \;<\; \frac{\lambda}{2} \tag{8}$$

where n_b and n_{ac} are the effective indices of the TE or TM modes in the narrow and wide sections, respectively. Intrinsically, for a strip waveguide well-supported TE mode, the effective index of TM mode is smaller than that of TE mode, and thereby once Eq. (1) is satisfied, Eq. (2) is also satisfied. Thus, the design process flow can be as follows: (1) use Bragg reflection regime condition to roughly estimate parameters of the photonic crystal; (2) simulate the k–ω diagrams for both TE and TM modes by the use of 3D FDTD; and (3) calculate the transmission responses for both TE and TM modes to further check the design. In Ref. [71], a measured extinction ratio of 40 dB was obtained with a period number of 40.

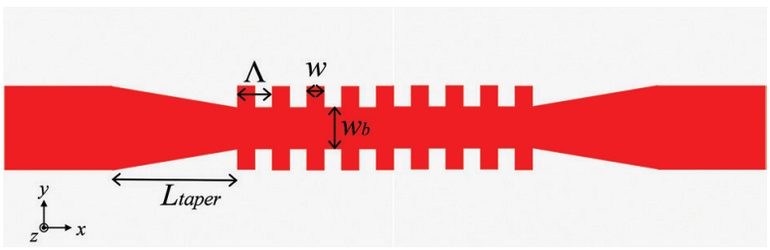

Figure 13. Schematic of a TM-pass polarizer assisted by 1D photonic crystals.

Adapting the same mechanism discussed above, higher-order mode pass filters have been demonstrated on a silicon wafer in Ref. [72], which are building blocks for mode-division multiplexing (MDM) systems. A 15.0-μm-long TE1 mode pass filter exhibits an extinction ratio of ~48 dB and an insertion loss of ~1.8 dB at 1550 nm.

6. Conclusion

1D photonic crystals have been well developed in silicon photonics and other material platforms as well. Three operating regimes allow 1D photonic crystals to be exploited in many different functional photonic devices with compact footprints. In diffraction regime, light beam can be diffracted into different directions by controlling configuration of photonic crystals in terms of pitch, duty cycle and effective index. In sub-wavelength regime, material refractive index, birefringence, and dispersion can be simply controlled by lithographic patterning to enable new design methods that lead to high-performance photonic devices. Propagation constant is proportional to operating wavelength and effective index in Bragg reflection regime. Thus, many wavelength-, mode-, and polarization-sensitive devices have been demonstrated with the assistance of Bragg gratings. In all these three regimes, when the operating wavelength range is fixed, the sub-wavelength gratings require tightest lithography process control that is high patterning resolution and is the most versatile one. Normally, sub-wavelength gratings are fabricated by electron-beam lithography which is not only expensive but also not suitable for mass production. And, the patterning resolution of DUV stepper lithography widely used in CMOS technology is not enough for accurately controlling sub-wavelength gratings. Therefore, continuing improvement in advanced lithography techniques is one important way to realize large-volume integration of sub-wavelength gratings with other electronic and photonic devices.

Author details

Liangshun Han

Address all correspondence to: liangshunhan@gmail.com

University of California, San Diego, USA

References

[1] Pantouvaki M et al. 50Gb/s Silicon Photonics Platform for Short-Reach Optical Interconnects, in Optical Fiber Communication Conference, OSA Technical Digest (online) (Optical Society of America, 2016), paper Th4H.4

[2] Heck MJR, Bowers JE. Energy efficient and energy proportional optical interconnects for multi-Core processors: Driving the need for on-Chip sources. IEEE Journal of Selected Topics in Quantum Electronics. Jul 2014;**20**(4):332-343

[3] Yu R et al. A scalable silicon photonic chip-scale optical switch for high performance computing systems. Optics Express. Dec 2013;**21**(26):32655

[4] Yang T et al. Experimental observation of optical differentiation and optical Hilbert transformation using a single SOI microdisk chip. Scientific Reports. Feb 2014;**4**:3960

[5] Juan-Colás J, Parkin A, Dunn KE, Scullion MG, Krauss TF, Johnson SD. The electrophotonic silicon biosensor. Nature Communications. Sep 2016;**7**:12769

[6] De Vos K, Bartolozzi I, Schacht E, Bienstman P, Baets R. Silicon-on-insulator microring resonator for sensitive and label-free biosensing. Optics Express. 2007;**15**(12):7610

[7] Chen S et al. Electrically pumped continuous-wave III–V quantum dot lasers on silicon. Nature Photonics. Mar 2016;**10**(5):307-311

[8] Duan G-H et al. Hybrid III–V on silicon lasers for photonic integrated circuits on silicon. IEEE Journal of Selected Topics in Quantum Electronics. Jul 2014;**20**(4):158-170

[9] Huolei W, Kim D, Harfouche M, Satyan N, Rakuljic G, and Yariv A. Narrow-Linewidth Oxide-Confined Heterogeneously Integrated Si/III-V Semiconductor Laser, in Conference on Lasers and Electro-Optics, OSA Technical Digest (online) (Optical Society of America, 2017), paper AM2B.2

[10] Thomson DJ et al. 50-Gb/s silicon optical modulator. IEEE Photonics Technology Letters. Feb 2012;**24**(4):234-236

[11] Xiao X et al. High-speed, low-loss silicon Mach–Zehnder modulators with doping optimization. Optics Express. Feb 2013;**21**(4):4116

[12] Novack A et al. Germanium photodetector with 60 GHz bandwidth using inductive gain peaking. Optics Express. Nov 2013;**21**(23):28387

[13] Lu L et al. 16 × 16 non-blocking silicon optical switch based on electro-optic Mach-Zehnder interferometers. Optics Express. May 2016;**24**(9):9295

[14] Tanizawa K et al. Ultra-compact 32 × 32 strictly-non-blocking Si-wire optical switch with fan-out LGA interposer. Optics Express. Jun 2015;**23**(13):17599

[15] Sun C et al. Single-chip microprocessor that communicates directly using light. Nature. Dec 2015;**528**(7583):534-538

[16] Joannopoulos JD, Johnson SG, Winn JN, Meade RD. Photonic Crystals: Molding the Flow of Light. Princeton, NJ: Princeton University Press; 2008

[17] Rytov SM. Electromagnetic properties of a finely stratified medium. Journal of Experimental and Theoretical Physics. 1956;**2**(3):466

[18] Tamir T, Peng ST. Analysis and design of grating couplers. Applied Physics. 1977;**14**(3): 235-254

[19] Chrostowski L, Hochberg M. Silicon Photonics Design. United Kingdom: Cambridge University Press; 2015

[20] Vermeulen D et al. High-efficiency fiber-to-chip grating couplers realized using an advanced CMOS-compatible silicon-on-insulator platform. Optics Express. Aug 2010; **18**(17):18278-18283

[21] Taillaert D et al. Grating couplers for coupling between optical fibers and Nanophotonic waveguides. Japanese Journal of Applied Physics. 2006;**45**(8R):6071

[22] Van Laere F et al. Compact focusing grating couplers for silicon-on-insulator integrated circuits. IEEE Photonics Technology Letters. 2007;**19**(23):1919-1921

[23] Waldhäusl R, Schnabel B, Dannberg P, Kley E-B, Bräuer A, Karthe W. Efficient coupling into polymer waveguides by gratings. Applied Optics. Dec 1997;**36**(36):9383-9390

[24] Van Laere F et al. Compact and highly efficient grating couplers between optical fiber and nanophotonic waveguides. Journal of Lightwave Technology. 2007;**25**(1):151-156

[25] Alonso-Ramos C, Zavargo-Peche L, Ortega-Moñux A, Halir R, Molina-Fernández I, Cheben P. Polarization-independent grating coupler for micrometric silicon rib waveguides. Optics Letters. Sep 2012;**37**(17):3663-3665

[26] Zaoui WS et al. Bridging the gap between optical fibers and silicon photonic integrated circuits. Optics Express. Jan 2014;**22**(2):1277-1286

[27] Taillaert D, Bienstman P, Baets R. Compact efficient broadband grating coupler for silicon-on-insulator waveguides. Optics Letters. Dec 2004;**29**(23):2749-2751

[28] Mekis A et al. A grating-coupler-enabled CMOS photonics platform. IEEE Journal of Selected Topics in Quantum Electronics. 2011;**17**(3):597-608

[29] Chen X, Li C, Fung CKY, Lo SMG, Tsang HK. Apodized waveguide grating couplers for efficient coupling to optical fibers. IEEE Photonics Technology Letters. 2010;**22**(15):1156-1158

[30] Ding Y, Ou H, Peucheret C. Ultrahigh-efficiency apodized grating coupler using fully etched photonic crystals. Optics Letters. 2013;**38**(15):2732-2734

[31] Chen X, Tsang HK. Polarization-independent grating couplers for silicon-on-insulator nanophotonic waveguides. Optics Letters. 2011;**36**(6):796-798

[32] Cheng Z, Tsang HK. Experimental demonstration of polarization-insensitive air-cladding grating couplers for silicon-on-insulator waveguides. Optics Letters. 2014; **39**(7):2206-2209

[33] Chen X, Xu K, Cheng Z, Fung CKY, Tsang HK. Wideband subwavelength gratings for coupling between silicon-on-insulator waveguides and optical fibers. Optics Letters. 2012;**37**(17):3483-3485

[34] Qin K et al. High efficiency and broadband two-dimensional blazed grating coupler with fully etched triangular holes. Journal of Lightwave Technology. 2012;**30**(14):2363-2366

[35] Cheben P et al. Refractive index engineering with subwavelength gratings for efficient microphotonic couplers and planar waveguide multiplexers. Optics Letters. 2010;**35**(15): 2526-2528

[36] Cheben P, Xu D-X, Janz S, Densmore A. Subwavelength waveguide grating for mode conversion and light coupling in integrated optics. Optics Express. 2006;**14**(11):4695-4702

[37] Almeida VR, Panepucci RR, Lipson M. Nanotaper for compact mode conversion. Optics Letters. 2003;**28**(15):1302-1304

[38] Bock PJ et al. Subwavelength grating periodic structures in silicon-on-insulator: A new type of microphotonic waveguide. Optics Express. 2010;**18**(19):20251-20262

[39] Bock PJ et al. Sub-wavelength grating mode transformers in silicon slab waveguides. Optics Express. 2009;**17**(21):19120-19133

[40] Ma Y et al. Ultralow loss single layer submicron silicon waveguide crossing for SOI optical interconnect. Optics Express. 2013;**21**(24):29374-29382

[41] Chen CH, Chiu CH. Taper-integrated multimode-interference based waveguide crossing design. IEEE Journal of Quantum Electronics. 2010;**46**(11):1656-1661

[42] Zhang Y, Hosseini A, Xu X, Kwong D, Chen RT. Ultralow-loss silicon waveguide crossing using Bloch modes in index-engineered cascaded multimode-interference couplers. Optics Letters. 2013;**38**(18):3608-3611

[43] Bock PJ et al. Subwavelength grating crossings for silicon wire waveguides. Optics Express. 2010;**18**(15):16146-16155

[44] Han L, Liang S, Zhu H, Zhang C, Wang W. A high extinction ratio polarization beam splitter with MMI couplers on InP substrate. IEEE Photonics Technology Letters. Apr 2015;**27**(7):782-785

[45] Han L, Liang S, Zhu H, Qiao L, Xu J, Wang W. Two-mode de/multiplexer based on multimode interference couplers with a tilted joint as phase shifter. Optics Letters. Feb 2015;**40**(4):518

[46] Han L, Liang S, Xu J, Qiao L, Zhu H, Wang W. Simultaneous wavelength- and mode-division (de)multiplexing for high-capacity on-Chip data transmission link. IEEE Photonics Journal. Apr 2016;**8**(2):1-10

[47] Soldano LB, Pennings ECM. Optical multi-mode interference devices based on self-imaging: Principles and applications. Journal of Lightwave Technology. 1995;**13**(4):615-627

[48] Halir R, Roelkens G, Ortega-Moñux A, Wangüemert-Pérez JG. High-performance 90° hybrid based on a silicon-on-insulator multimode interference coupler. Optics Letters. 2011;**36**(2):178-180

[49] Ortega-Monux A et al. High-performance multimode interference coupler in silicon waveguides with subwavelength structures. IEEE Photonics Technology Letters. 2011;**23**(19): 1406-1408

[50] Maese-Novo A et al. Wavelength independent multimode interference coupler. Optics Express. 2013;**21**(6):7033-7040

[51] Halir R et al. Colorless directional coupler with dispersion engineered sub-wavelength structure. Optics Express. 2012;**20**(12):13470-13477

[52] Cheng N-C, Ma Y-F, Fu P-H, Chin C-C, Huang D-W. Horizontal slot waveguides for polarization branching control. Applied Optics. 2015;**54**(3):436-443

[53] Alam MZ, Aitchison JS, Mojahedi M. Polarization-independent hybrid plasmonic coupler for a silicon on insulator platform. Optics Letters. 2012;**37**(16):3417-3419

[54] Xiao J, Liu X, Sun X. Design of polarization-independent optical couplers composed of three parallel slot waveguides. Applied Optics. 2008;**47**(14):2687-2695

[55] Liu L, Deng Q, Zhou Z. Subwavelength-grating-assisted broadband polarization-independent directional coupler. Optics Letters. 2016;**41**(7):1648-1651

[56] Han L et al. DBR laser with over 20 nm wavelength tuning range. IEEE Photonics Technology Letters. 2016:1-1

[57] Han L et al. Electroabsorption-modulated widely tunable DBR laser transmitter for WDM-PONs. Optics Express. Dec 2014;**22**(24):30368

[58] Zhang C, Liang S, Zhu H, Han L, Wang W. Multichannel DFB laser arrays fabricated by upper SCH layer SAG technique. IEEE Journal of Quantum Electronics. Feb 2014;**50**(2): 92-97

[59] Hou L, Xu J, Eddie I, Han L, Zhu H, and Marsh J. DWDM Source Based on Monolithic Side-Wall Sample Grating DFB Laser Array, in Conference on Lasers and Electro-Optics, OSA Technical Digest (2016) (Optical Society of America, 2016), paper SW4M.1

[60] Kashyap R. Fiber Bragg Grating. San Diego: Academic Press; 1999

[61] Jewell JL, Harbison JP, Scherer A, Lee YH, Florez LT. Vertical-cavity surface-emitting lasers: Design, growth, fabrication, characterization. IEEE Journal of Quantum Electronics. 1991;**27**(6):1332-1346

[62] Roth JE, Palermo S, Helman NC, Bour DP, Miller DA, and Horowitz M. 1550nm Optical Interconnect Transceiver with Low Voltage Electroabsorption Modulators Flip-Chip Bonded to 90nm CMOS, in Optical Fiber Communication Conference and Exposition and The National Fiber Optic Engineers Conference, OSA Technical Digest Series (CD) (Optical Society of America, 2007), paper JThA38

[63] Kreissl J, Bornholdt C, Gaertner T, Moerl L, Przyrembel G, Rehbein W. 1550 nm flip-chip compatible electroabsorption-modulated laser with 40 Gb/s modulation capability. In: IPRM 2011 – 23rd International Conference on Indium Phosphide and Related Materials (IEEE, 2011); pp. 1-4

[64] Roelkens G, Brouckaert J, Van Thourhout D, Baets R, Nötzel R, Smit M. Adhesive bonding of InP/InGaAsP dies to processed silicon-on-insulator wafers using DVS-bis-Benzocyclobutene. Journal of the Electrochemical Society. 2006;**153**(12):G1015

[65] Liang D, Roelkens G, Baets R, Bowers JE. Hybrid integrated platforms for silicon photonics. Materials (Basel). 2010;**3**(3):1782-1802

[66] Tao L et al. 4-λ InGaAsP-Si distributed feedback evanescent lasers with varying silicon waveguide width. Optics Express. Mar 2014;**22**(5):5448

[67] Dai D, Bowers JE. Novel concept for ultracompact polarization splitter-rotator based on silicon nanowires. Optics Express. May 2011;**19**(11):10940

[68] Alam MZ, Aitchison JS, Mojahedi M. Compact and silicon-on-insulator-compatible hybrid plasmonic TE-pass polarizer. Optics Letters. 2012;**37**(1):55-57

[69] Avrutsky I. Integrated optical polarizer for silicon-on-insulator waveguides using evanescent wave coupling to gap plasmon-polaritons. IEEE Journal of Selected Topics in Quantum Electronics. 2008;**14**(6):1509-1514

[70] Dai D, Wang Z, Julian N, Bowers JE. Compact broadband polarizer based on shallowly-etched silicon-on-insulator ridge optical waveguides. Optics Express. 2010;**18**(26): 27404-27415

[71] Guan X, Chen P, Chen S, Xu P, Shi Y, Dai D. Low-loss ultracompact transverse-magnetic-pass polarizer with a silicon subwavelength grating waveguide. Optics Letters. 2014;**39**(15):4514-4517

[72] Guan X, Ding Y, Frandsen LH. Ultra-compact broadband higher order-mode pass filter fabricated in a silicon waveguide for multimode photonics. Optics Letters. 2015;**40**(16): 3893-3896